

# Fabrication of Electrically Conductive Metal Patterns at the Surface of Polymer Films by Microplasma-Based Direct Writing

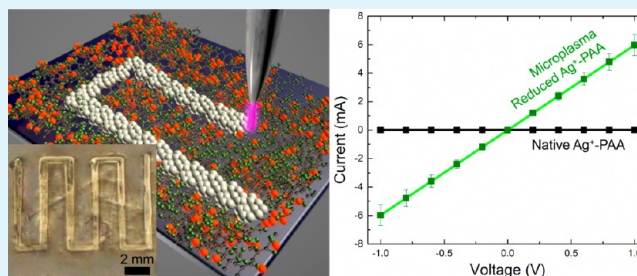
Souvik Ghosh,<sup>†</sup> Rui Yang,<sup>‡</sup> Michelle Kaumeyer,<sup>‡</sup> Christian A. Zorman,<sup>‡</sup> Stuart J. Rowan,<sup>§</sup> Philip X.-L. Feng,<sup>‡</sup> and R. Mohan Sankaran<sup>\*,†</sup>

<sup>†</sup>Department of Chemical Engineering, <sup>‡</sup>Department of Electrical Engineering and Computer Science, and <sup>§</sup>Department of Macromolecular Sciences and Engineering, Case Western Reserve University, Cleveland, Ohio, United States

## Supporting Information

**ABSTRACT:** We describe a direct-write process for producing electrically conductive metal patterns at the surface of polymers. Thin films of poly(acrylic acid) (PAA) loaded with Ag ions are reduced by a scanning, atmospheric-pressure microplasma to form crystalline Ag features with a line width of 300  $\mu\text{m}$ . Materials analysis reveals that the metallization occurs in a thin layer of  $\sim 5 \mu\text{m}$  near the film surface, suggesting that the Ag ions diffuse to the surface. Sheet resistances of 1–10  $\Omega/\text{sq}$  are obtained independent of film thickness and Ag volume concentration, which is desirable for producing surface conductivity on polymers while minimizing metal loading.

**KEYWORDS:** microplasma, direct write, electrodiffusion, printed electronics, flexible electronics, sheet resistance



## INTRODUCTION

Patterning metal as a contact or interconnect is a critical processing step for device fabrication in a wide range of applications. Traditionally, physical vapor deposition (PVD) is combined with lithography to first deposit a metal film such as Ag, then remove the undesired areas to produce a pattern. Although this subtractive approach has high fidelity and results in an electrically conductive metal layer without any thermal annealing, the low throughput, materials wastage, and need for vacuum lead to high operating costs and limited scalability.<sup>1</sup> Recently, the emergence of flexible electronic devices has stimulated the desire for alternative, additive approaches for fabricating patterned metal features. Some examples of techniques that have been developed include inkjet printing,<sup>2,3</sup> screen printing,<sup>4,5</sup> aerosol printing,<sup>6,7</sup> and nanoimprint lithography.<sup>8,9</sup> A common feature of these processes is the inks, which typically comprise organic-ligand stabilized dispersions of metal nanoparticles<sup>2</sup> or metal–organic compounds.<sup>3,10,11</sup> An advantage of ink-based printing methods is that the processes are carried out at ambient conditions and therefore can be easily integrated with roll-to-roll systems for large-scale manufacturing.<sup>1,12</sup> However, the inks themselves are usually expensive due to the number of processing steps associated with synthesis, dispersion, purification, and concentration. In addition, the as-deposited films often exhibit poor conductivity requiring a postdeposition annealing step, which may not be compatible with some polymer substrates.<sup>13</sup> Highly conductive films have been produced at room temperature by electroless deposition where the metal is chemically reduced onto a polymeric substrate from solution.<sup>14–16</sup> Electroless processes require an initial metal layer that is often prepared by

inkjet printing to serve as activation sites and obtain patterned deposits.<sup>17,18</sup> Alternatively, patterns of metallic features have been directly written by exposing polymer films containing a metal precursor to a laser<sup>19,20</sup> or electron beam.<sup>21</sup> Unfortunately, these processes remain complex and in many cases require annealing to produce reasonable conductivity.

Here, we present a direct-write process at ambient conditions to produce electrically conductive metal patterns at the surface of polymer films. The process bears similarities with electron-beam assisted nanofabrication, but does not require vacuum, postannealing, or complex equipment. Polymer films are first prepared with a metal phase and then exposed to a scanning, nonthermal, atmospheric-pressure microplasma. Localized reactions between the electrons in the microplasma and metal ions in the film result in reduction, nanoparticle nucleation and growth, and aggregation of the nanoparticles into a percolating network of electrically conductive metal particles. A particularly unique aspect of the process is that the metallization occurs near the film surface which we propose occurs via electrodiffusion of the metal ions in the electric field created by the microplasma. Thus, highly conductive films with a sheet resistance as low as 1  $\Omega/\text{sq}$  are produced at relatively low metal loading in the polymer film.

## EXPERIMENTAL PROCEDURE

Thin films of poly(acrylic acid) (PAA) loaded with silver cations ( $\text{Ag}^+$ ) were prepared by solution methods. PAA (Acros

Received: December 27, 2013

Accepted: February 20, 2014

Published: February 20, 2014

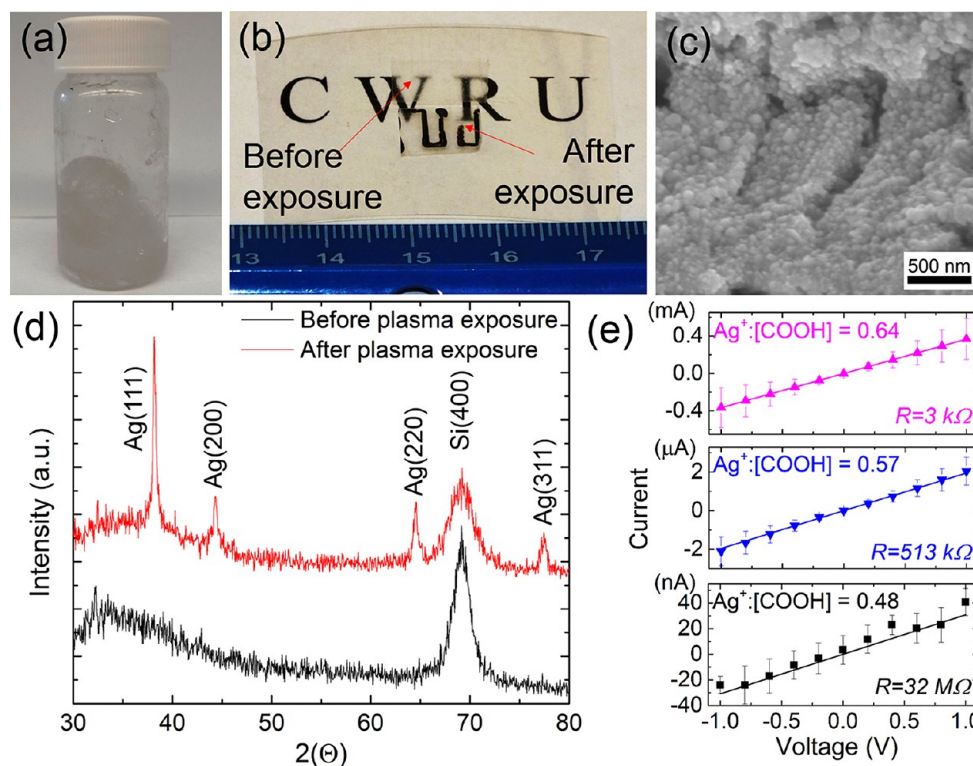


**Figure 1.** (a) Optical image of Ag/PAA after formation of gel precipitate ( $\text{Ag}^+:[\text{COOH}] = 0.64:1$ ). (b) Optical images of Ag/PAA films on a PET sheet with the letters “CWRU” behind on paper, before and after microplasma exposure. The films were transferred by peeling off the Si substrate. (c) SEM image of microstructure of Ag/PAA film ( $\text{Ag}^+:[\text{COOH}] = 0.64:1$ ) showing network of Ag particles after microplasma reduction. (d) XRD of Ag/PAA films ( $\text{Ag}^+:[\text{COOH}] = 0.64:1$ ) showing the formation of crystalline Ag after microplasma exposure. (e) Current–voltage characteristics of microplasma-reduced lines, each  $300 \mu\text{m} \times 5 \text{ mm}$ , on  $8 \mu\text{m}$  thick films as a function of the  $\text{Ag}^+:[\text{COOH}]$  ratio.

Organic,  $M_w = 1\,260\,000$ ) was dissolved in 100 mL of 1:3 v/v deionized water:ethanol at 0.255% w/v. Silver nitrate ( $\text{AgNO}_3$ , >99.9% purity, Alfa Aesar) dissolved in 20 mL of the same solvent was added to the solution and stirred vigorously for 10 min. An additional 150 mL of ethanol was then added to this mixture and left to stir for another 15 min. The resultant milky white solution was centrifuged and a white precipitate containing the PAA and  $\text{Ag}^+$  was collected after decanting the clear supernatant. The precipitate was homogenized in 6:1 v/v water:ethylene glycol at 10–20% w/w (Cole Parmer, LabGen 7). After homogenizing, the sample was kept in vacuum (approximately  $-20 \text{ psi}$ ) for a minute to remove air bubbles. The resulting fluid was cast with a doctor’s blade on n-type silicon (Si) (100) wafers, dried overnight, and finally vacuum-dried for 2 h before microplasma exposure. The Ag concentration in the deposited film was calculated as the molar ratio of  $\text{Ag}^+$  to repeat units of PAA, i.e.,  $(\text{CH}(\text{COOH})\text{-CH}_2)$ , represented as  $[\text{COOH}]$ , in the solution. For example, a film containing  $\text{Ag}^+:[\text{COOH}] = 1:1$  indicates that 169.87 g of  $\text{AgNO}_3$  was mixed with 72 g of PAA in solution.

Patterns of reduced Ag were fabricated by exposing the Ag/PAA film to a scanning, nonthermal, atmospheric-pressure microplasma. Details of the microplasma setup are described elsewhere.<sup>22,23</sup> Here, we formed a microplasma in a flow of argon (Ar) gas at 700 V and 1 mA with a cathode to anode gap of  $500 \mu\text{m}$ . The microplasma was scanned across the film by moving the substrate in two dimensions with a pair of computer-controlled stepper motors. A minimum average line width of  $300 \mu\text{m}$  was obtained at a scan rate of  $250 \mu\text{m/s}$  (see the Supporting Information).

After microplasma exposure, the processed film was peeled off from the Si substrate and placed on an insulating substrate such as glass or polyethylene terephthalate (PET). Conductive Ag paste was used to deposit contact pads on the microplasma-reduced features for current–voltage ( $I$ – $V$ ) measurements. Electrical characterization was performed inside a Faraday chamber with a two-point probe setup using a Keithley 4200 SCS source which can precisely measure resistances ranging from  $1 \times 10^{-6}$  to  $1 \times 10^{12} \Omega$ .

Scanning electron microscopy (SEM), focused ion beam (FIB) etching, and energy dispersive spectroscopy (EDX) were performed with a FEI Nova Nanolab 200 field-emission gun SEM. The polymer samples were sputter coated with 5 nm Pd prior to SEM.

## RESULTS AND DISCUSSION

A key part of this study was the selection of the metal (and corresponding metal precursor) and polymer to be exposed to the scanning microplasma process to obtain electrically conductive patterns. We focused on water-soluble metal salts and polymers that are widely used, safe, low cost, and easy to solution process. We chose Ag as the metal because it is an excellent conductor, easy to reduce [standard reduction potential = 0.799 V vs standard hydrogen electrode (SHE)], is significantly less expensive than other metals such as Au, and has a readily available water-soluble salt,  $\text{AgNO}_3$ . Polyacrylic acid (PAA) was selected as the polymer because it is also water-soluble, and has been previously reported to electrostatically bind with different metal cations, including  $\text{Ag}^+$ , through its carboxylic acid ( $-\text{COOH}$ ) side chains.<sup>24–26</sup> After loading, the

solubility in polar solvents is reduced, facilitating recovery of the metal ion-polymer mixture. Figure 1a shows an image of the Ag/PAA gel precipitate after separation from the supernatant. Casting using a doctor's blade produces a semitransparent film containing only the polymer and  $\text{Ag}^+$  (Figure 1b). Exposing to the microplasma results in a clear color change attributed to the formation of metallic Ag at the surface of the film (Figure 1b). A representative scanning electron microscope (SEM) image of a patterned line on a film containing  $\text{Ag}^+:[\text{COOH}] = 0.64$  reveals the presence of particles within the feature, presumably Ag, forming a relatively uniform and continuous network (Figure 1c). X-ray diffraction (XRD) confirmed that the patterned line consisted of crystalline Ag [Figure 1(d)]. We similarly prepared 5  $\mu\text{m}$  thick Ag/PAA films containing different ratios of  $\text{Ag}^+:[\text{COOH}]$  ranging from 0.32:1 to 0.64:1. Figure 1e shows I–V characteristics of the 5 mm long patterned lines produced upon exposure to plasma. With increasing concentration of  $\text{Ag}^+$  in the polymer, the resistances determined from the average slope were found to decrease from 32  $\text{M}\Omega$  to 3  $\text{k}\Omega$ , consistent with higher  $\text{Ag}^+:[\text{COOH}]$  ratios leading to more conductive networks.

To further examine the microplasma-reduced lines and understand the nature of particle formation and conductivity, we carried out additional SEM and energy-dispersive spectroscopic (EDX) analyses. Images a and b in Figure 2 show SEM images and corresponding EDX maps of lines patterned in a relatively low Ag concentration ( $\text{Ag}^+:[\text{COOH}] = 0.32:1$ ) film by the microplasma. The EDX maps are also colored with the intensity corresponding to the Ag content in the film. The high intensity of Ag confirms that Ag ions are reduced, leading to particle nucleation and growth in the patterned region [Figure 2(b)]. In order to analyze the concentration of Ag within the film, a 5  $\mu\text{m}$  deep trench was created across the patterned line by focused ion beam (FIB). The EDX map suggests that the Ag concentration is higher near the surface [Figure 2(b)]. To more carefully characterize the concentration depth profile, films were cut and SEM images and corresponding EDX false color intensity maps were obtained (Figure 2c–h). The cross-sectional analysis shows high surface concentration of Ag, confirming that the reduction and formation of Ag particles is localized near the surface (Figure 2c, d). This is further supported by images near the edge of a patterned line that show the nonuniform Ag concentration only occurs in the exposed part of the film (Figure 2e, f). Images of the unexposed region of the same film show that without plasma exposure, the Ag ion concentration is homogeneous throughout the film depth (Figure 2g, h). The cross-sectional images were semiquantitatively analyzed by plotting the intensity of the EDX line scan as a function of film depth (Figure 3). SEM images of the EDX scan areas are also shown in Figure 3 for reference. We find that in the native film, the Ag and C concentrations are constant throughout the film at an atomic percent of 25 at % Ag and 50 at % C. The Ag concentration rapidly increases after microplasma exposure at the film surface to  $\sim 75$  at %, and, simultaneously, the C concentration decreases to  $\sim 25$  at %. Moving down from the film surface, the Ag concentration rapidly decreases from 75 at % at  $\sim 5$   $\mu\text{m}$  and reaches its original value of 25 at % at a depth of  $\sim 10$   $\mu\text{m}$ . Near the base of the film, the C concentration increases to  $\sim 75$  at % and the Ag concentration is depleted to  $\sim 10$  at %.

The enrichment of Ag at the surface and simultaneous depletion of Ag at the base of the film after microplasma

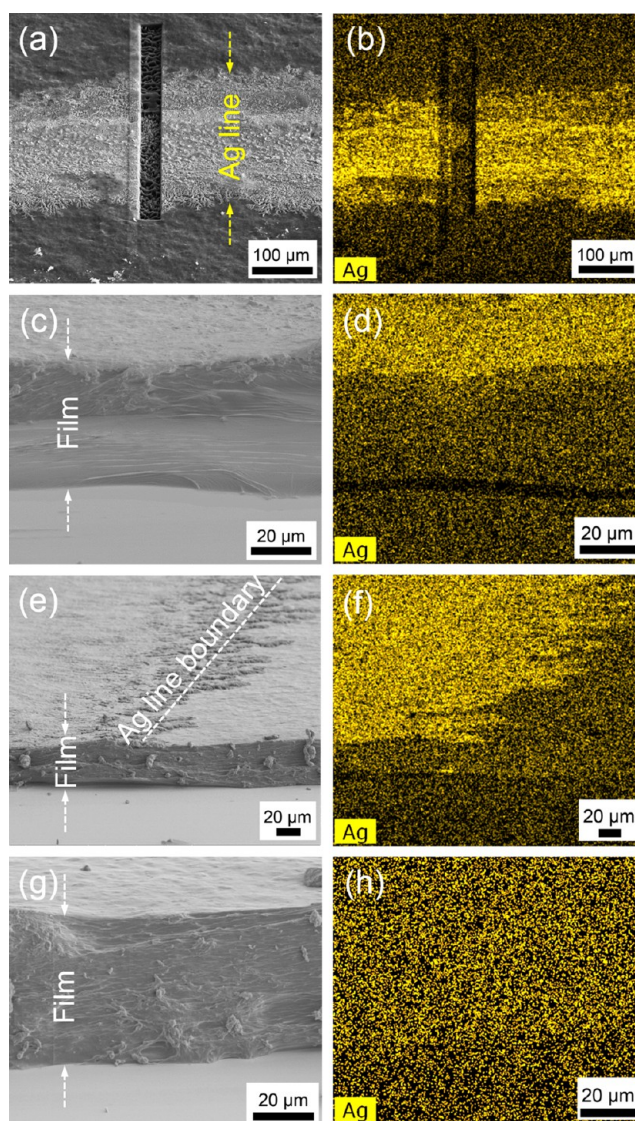


**Figure 2.** (a) The center of the Ag line was etched by FIB. The center of the line was etched by FIB. (b) EDX false color map of Ag in a. (c) Cross-sectional SEM image of microplasma-reduced region. (d) EDX false color map of Ag in c showing higher concentration of Ag at the surface. (e) Cross-sectional SEM image at the boundary of a microplasma-reduced line. (f) EDX false color map of Ag in (e) showing higher surface concentration of Ag only in the microplasma exposed region. (g) Cross-sectional SEM image of an unexposed region of the same sample analyzed in c–f. (h) EDX false color map of Ag in g showing uniform distribution of Ag.

exposure suggest that surface reduction alone cannot explain the formation of an Ag-rich surface layer. We propose that Ag ions within the bulk of the film diffuse to the surface during microplasma exposure to supply metal precursor for continued growth. The DC microplasma process produces an electric field within the film oriented with a negative pole at the surface and a positive pole at the base. This electric field may drive diffusion of the positively charged  $\text{Ag}^+$  to the film surface, termed electrodiffusion.<sup>27</sup> The coordination of  $\text{Ag}^+$  to PAA is reversible<sup>25</sup> and the electric field should present a strong enough force to pull the  $\text{Ag}^+$  ions to the film surface where they can undergo reduction by electrons from the microplasma. It is possible that the polymer may undergo some morphological changes during this process; however it still acts as a supporting

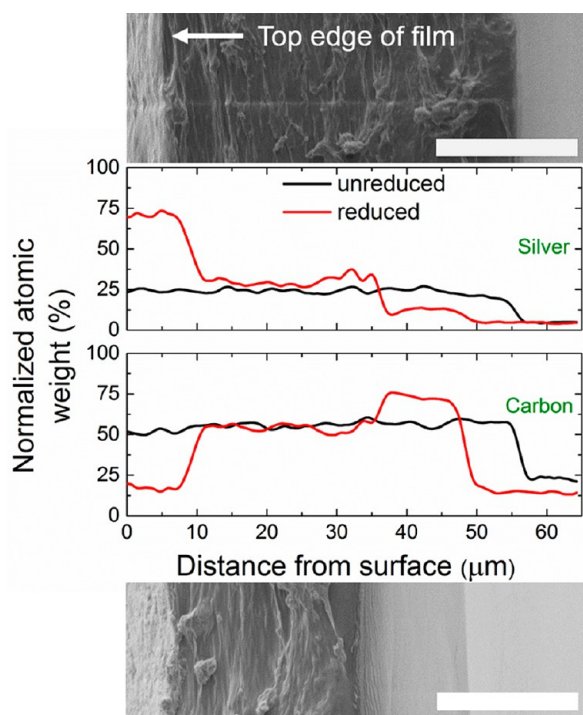


**Figure 3.** Cross-sectional SEM images of Ag/PAA films before (top) and after (bottom) microplasma reduction and corresponding normalized atomic weight of Ag and C through the film depth, as obtained by EDX line scans. Scale bar is  $20\ \mu\text{m}$ .

backbone to the Ag layer on the surface. To validate this qualitative picture, we processed films of varying thickness with a low Ag content ( $\text{Ag}^+:\text{[COOH]} = 0.32:1$ ). If electrodiffusion of Ag ions occurs during microplasma exposure, thicker films should provide a larger reservoir for particle growth, and thus form Ag lines with lower resistance. Figure 4(a) shows that by increasing the thickness from 3 to  $20\ \mu\text{m}$ , the resistance of a constant line shape of  $300\ \mu\text{m} \times 5\ \text{mm}$  decreases from approximately  $30\ \text{M}\Omega$  to  $200\ \Omega$ , supporting the electrodiffusion model. Consistent with this picture, the resistance on the back of the films remains high (see the Supporting Information). We also carried out several control experiments and found that neither UV light from the microplasma nor other UV sources could produce the same reduced metallic films (see the Supporting Information). This further underscores the importance of electrodiffusion which we believe is critical to the precipitation of a metallic, conductive Ag layer in our films.

The figure of merit for electrical conductivity is bulk resistivity. Bulk resistivity can be calculated from the geometry of the microplasma drawn line. The thickness of our reduced lines is not the original film thickness, but some surface layer that is on the order of  $\sim 5\ \mu\text{m}$  thick, based on cross-sectional EDX analysis (see Figure 3). Assuming this thickness, we estimated a bulk conductivity of  $4.5\ \text{m}\Omega\ \text{cm}$  for films containing a  $\text{Ag}^+:\text{[COOH]}$  ratio of 0.32. However, the concentration of Ag in this layer is not constant and decreases moving away from the surface into the bulk of the film. Because the Ag concentration is significantly higher in this near surface region than the rest of the film, we can assume that the surface layer is the primary contributor to electrical conduction and characterize the film conductivity by the sheet resistance. Figure 4b shows sheet resistances as a function of the original film thickness after microplasma exposure for two difference ratios

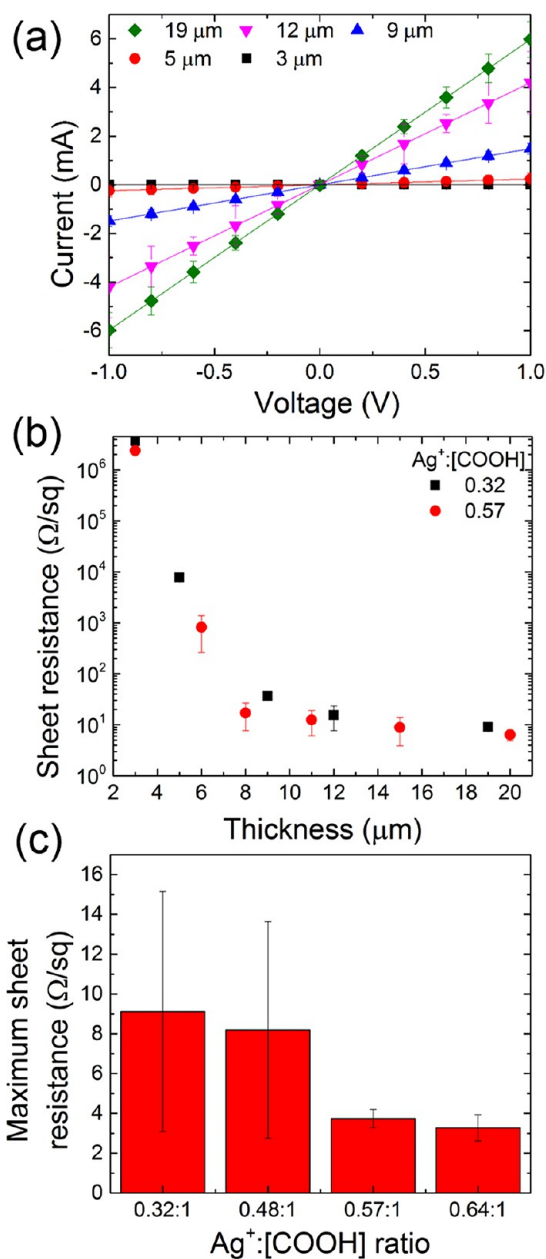


**Figure 4.** (a) Current–voltage characteristics of  $5000 \times 300\ \mu\text{m}^2$  microplasma-reduced lines in  $\text{Ag}^+:\text{[COOH]} = 0.32:1$  films of varying thickness. The data were fitted by linear regression with a y-intercept of 0 to yield ohmic resistances of  $35\ \text{M}\Omega$ ,  $4\ \text{k}\Omega$ ,  $671\ \Omega$ ,  $238\ \Omega$ , and  $167\ \Omega$  for original film thicknesses of 3, 5, 9, 12, and  $19\ \mu\text{m}$  respectively. (b) Average sheet resistance as a function of original film thickness at two concentrations of  $\text{Ag}^+:\text{[COOH]}$ . (c) Maximum average sheet resistance for films of different  $\text{Ag}^+:\text{[COOH]}$  concentrations. All films had original thicknesses  $>20\ \mu\text{m}$ .

of  $\text{Ag}^+:\text{[COOH]}$ . For thin films ( $<10\ \mu\text{m}$ ), the Ag loading in the film volume or the exposure time (scanning rate) is too low for the Ag to diffuse to the surface and react to form a percolated network. Beyond a critical thickness of approximately  $\sim 12\ \mu\text{m}$ , the sheet resistance of the microplasma-reduced lines decreases dramatically and becomes independent of the film thickness ( $\sim 10\ \Omega/\text{sq}$ ), indicating that the Ag loading is high enough to diffuse within the time scale of microplasma exposure to form a percolated network. These results indicate that the sheet resistance reaches a maximum at

a sufficiently large film thickness, independent of the initial  $\text{Ag}^+$ : $[\text{COOH}]$  concentration. Thus, the sheet resistance can be optimized for any given  $\text{Ag}^+$ : $[\text{COOH}]$  concentration. Figure 4c shows the maximum sheet resistance obtained on films with  $\text{Ag}^+$ : $[\text{COOH}]$  ratios of 0.32:1, 0.48:1, 0.57:1 and 0.64:1, respectively, and thicknesses  $>20 \mu\text{m}$ . The sheet resistances are found to be between 1 and  $10 \Omega/\text{sq}$ , independent of Ag loading. These values are comparable to Ag features obtained by inkjet printing ( $38 \Omega/\text{sq}$ ), screen printing ( $\sim 50 \text{ m}\Omega/\text{sq}$ ),<sup>12,28</sup> spray deposition ( $\sim 50 \Omega/\text{sq}$ ),<sup>29</sup> and electroless deposition ( $\sim 0.1 \text{ m}\Omega/\text{sq}$ ).<sup>30</sup>

## CONCLUSIONS

In summary, we have developed a room condition, direct-write process based on a scanning, atmospheric-pressure microplasma to produce electrically conductive lines at the surface of polymer films. Our study suggests that the metallization occurs via electrodiffusion of Ag ions to the film surface and reduction by the microplasma. The surface conductivity is maximized independent of metal loading, which may be desirable to reduce overall metal content while producing conductivity where it is desirable for many flexible conductor applications, at the surface of the film.

## ASSOCIATED CONTENT

### Supporting Information

Additional experimental details, materials characterization, electrical measurements, and control experiments with UV sources. This material is available free of charge via the Internet at <http://pubs.acs.org>.

## AUTHOR INFORMATION

### Corresponding Author

\*E-mail: [mohan@case.edu](mailto:mohan@case.edu).

### Notes

The authors declare no competing financial interest.

## ACKNOWLEDGMENTS

This work was supported by the National Science Foundation (NSF) Grant SNM-1246715. The authors acknowledge Laurie Dudik (Managing Engineer, Electronics Design Center, Case Western Reserve University) for help with the homogenizer and doctor-blade casting techniques, Dr. Ina Martin (Director, Materials for Opto-electronics Research and Education Center, Case Western Reserve University) for assistance with surface profilometry, and Prof. Harihara Baskaran (Department of Chemical Engineering, Case Western Reserve University) for access to a TCSC Centrifuge.

## REFERENCES

- (1) Forrest, S. R. The Path to Ubiquitous and Low-Cost Organic Electronic Appliances on Plastic. *Nature* **2004**, *428*, 911–918.
- (2) Russo, A.; Ahn, B. Y.; Adams, J. J.; Duoss, E. B.; Bernhard, J. T.; Lewis, J. A. Pen-on-Paper Flexible Electronics. *Adv. Mater.* **2011**, *23*, 3426–3430.
- (3) Walker, S. B.; Lewis, J. A. Reactive Silver Inks for Patterning High-Conductivity Features at Mild Temperatures. *J. Am. Chem. Soc.* **2012**, *134*, 1419–1421.
- (4) Faddoul, R.; Reverdy-Bruas, N.; Blayo, A. Formulation and Screen Printing of Water Based Conductive Flake Silver Pastes Onto Green Ceramic Tapes for Electronic Applications. *Mater. Sci. Eng., B* **2012**, *177*, 1053–1066.

- (5) Zhang, Y.; Zhu, P.; Li, G.; Zhao, T.; Fu, X.; Sun, R.; Zhou, F.; Wong, C.-P. Facile Preparation of Monodisperse, Impurity-Free, and Antioxidation Copper Nanoparticles on a Large Scale for Application in Conductive Ink. *ACS Appl. Mater. Interfaces* **2014**, *6*, 560–567.

- (6) Zhao, D.; Liu, T.; Zhang, M.; Liang, R.; Wang, B. Fabrication and Characterization of Aerosol-Jet Printed Strain Sensors for Multifunctional Composite Structures. *Smart Mater. Struct.* **2012**, *21*, 115008.

- (7) Mahajan, A.; Frisbie, C. D.; Francis, L. F. Optimization of Aerosol Jet Printing for High-Resolution, High-Aspect Ratio Silver Lines. *ACS Appl. Mater. Interfaces* **2013**, *5*, 4856–4864.

- (8) Ok, J. G.; Kwak, M. K.; Huard, C. M.; Youn, H. S.; Guo, L. J. Photo-Roll Lithography (PRL) for Continuous and Scalable Patterning with Application in Flexible Electronics. *Adv. Mater.* **2013**, *25*, 6554–6561.

- (9) Ahn, S. H.; Guo, L. J. Large-Area Roll-to-Roll and Roll-to-Plate Nanoimprint Lithography: A Step toward High-Throughput Application of Continuous Nanoimprinting. *ACS Nano* **2009**, *3*, 2304–2310.

- (10) Jahn, S. F.; Blaudeck, T.; Baumann, R. R.; Jakob, A.; Ecorchard, P.; Ruffer, T.; Lang, H.; Schmidt, P. Inkjet Printing of Conductive Silver Patterns by Using the First-Aqueous Particle-Free MOD Ink without Additional Stabilizing Ligands. *Chem. Mater.* **2010**, *22*, 3067–3071.

- (11) Komoda, N.; Nogi, M.; Suganuma, K.; Otsuka, K. Highly Sensitive Antenna Using Inkjet Overprinting with Particle-Free Conductive Inks. *ACS Appl. Mater. Interfaces* **2012**, *4*, 5732–5736.

- (12) Hosel, M.; Sondergaard, R. R.; Angmo, D.; Krebs, F. C. Comparison of Fast Roll-to-Roll Flexographic, Inkjet, Flatbed, and Rotary Screen Printing of Metal Back Electrodes for Polymer Solar Cells. *Adv. Eng. Mater.* **2013**, *15*, 995–1001.

- (13) Perelaer, J.; Smith, P. J.; Mager, D.; Soltman, D.; Volkman, S. K.; Subramanian, V.; Korvink, J. G.; Schubert, U. S. Printed Electronics: The Challenges Involved in Printing Devices, Interconnects, and Contacts Based on Inorganic Materials. *J. Mater. Chem.* **2010**, *20*, 8446–8453.

- (14) Bessueille, F.; Gout, S.; Cotte, S.; Goepfert, Y.; Leonard, D.; Romand, M. Selective Metal Pattern Fabrication Through Micro-Contact or Ink-Jet Printing and Electroless Plating onto Polymer Surfaces Chemically Modified by Plasma Treatments. *J. Adhes.* **2009**, *85*, 690–710.

- (15) Wolf, S.; Feldmann, C.  $\text{Cu}_2\text{X}(\text{OH})_3$  ( $\text{X} = \text{Cl}^-, \text{NO}_3^-$ ): Synthesis of Nanoparticles and Its Application for Room Temperature Deposition/Printing of Conductive Copper Thin-Films. *J. Mater. Chem.* **2010**, *20*, 7694–7699.

- (16) Liao, Y.-C.; Kao, Z.-K. Direct Writing Patterns for Electroless Plated Copper Thin Film on Plastic Substrates. *ACS Appl. Mater. Interfaces* **2012**, *4*, 5109–5113.

- (17) Cheng, K.; Yang, M.-W.; Chiu, W. W. W.; Huang, C.-Y.; Chang, J.; Ying, T.-F.; Yang, Y. Ink-Jet Printing, Self-Assembled Polyelectrolytes, and Electroless Plating: Low Cost Fabrication of Circuits on a Flexible Substrate at Room Temperature. *Macromol. Rapid Commun.* **2005**, *26*, 247–264.

- (18) Garcia, A.; Polesel-Maris, J.; Viel, P.; Palacin, S.; Berthelot, T. Localized Ligand Induced Electroless Plating (LIEP) Process for the Fabrication of Copper Patterns Onto Flexible Polymer Substrates. *Adv. Funct. Mater.* **2011**, *21*, 2096–2102.

- (19) Stellacci, F.; Batter, C. A. Laser and Electron-Beam Induced Growth of Nanoparticles for 2D and 3D Metal Patterning. *Adv. Mater.* **2002**, *14*, 194–198.

- (20) Maruo, S.; Fourkas, J. T. Recent Progress in Multiphoton Microfabrication. *Laser Photon. Rev.* **2008**, *2*, 100–111.

- (21) Radha, B.; Kiruthika, S.; Kulkarni, G. U. Metal Anion-Alkyl Ammonium Complexes as Direct Write Precursors to Produce Nanopatterns of Metals, Nitrides, Oxides, Sulfides, and Alloys. *J. Am. Chem. Soc.* **2011**, *133*, 12706–12713.

- (22) Richmonds, C.; Sankaran, R. M. Plasma-Liquid Electrochemistry: Rapid Synthesis of Colloidal Metal Nanoparticles by Microplasma Reduction of Aqueous Cations. *Appl. Phys. Lett.* **2008**, *93*, 131501–03.

(23) Lee, S. W.; Kumpfer, J. K.; Lin, P. A.; Li, G.; Gao, X. P. A.; Rowan, S. J.; Sankaran, R. M. In Situ Formation of Metal Nanoparticle Composites Via “Soft” Plasma Electrochemical Reduction of Metallosupramolecular Polymer Films. *Macromolecules* **2012**, *45*, 8201–8210.

(24) Zhang, W.; Zhang, A.; Guan, Y.; Zhang, Y.; Zhu, X. X. Silver-Loading in Uncrosslinked Hydrogen-Bonded Lbl Films: Structure Change and Improved Stability. *J. Mater. Chem.* **2011**, *21*, 548–555.

(25) Lahav, M.; Narovlyansky, M.; Winkleman, A.; Perez-Castillejos, R.; Weiss, E. A.; Whitesides, G. A. Patterning of Poly(acrylic acid) by Ionic Exchange Reactions in Microfluidic Channels. *Adv. Mater.* **2006**, *18*, 3174–3178.

(26) Winkleman, A.; Perez-Castillejos, R.; Lahav, M.; Narovlyansky, M.; Rodriguez, L. N. J.; Whitesides, G. M. Patterning Micron-Sized Features in a Cross-Linked Poly(Acrylic Acid) Film by a Wet Etching Process. *Soft Matter* **2007**, *3*, 108–116.

(27) Lebedev, E. A.; Süptitz, P.; Willert, I. Transport of Silver Under the Influence of an Electric Field in Glassy As<sub>2</sub>Se<sub>3</sub>. *Phys. Status Solidi (a)* **2006**, *28*, 461–466.

(28) Nge, T. T.; Nogi, M.; Suganuma, K. Electrical Functionality of Inkjet-Printed Silver Nanoparticle Conductive Tracks on Nanostructured Paper Compared with Those on Plastic Substrates. *J. Mater. Chem. C* **2013**, *1*, 5235–5243.

(29) Scardaci, V.; Coull, R.; Lyons, P. E.; Rickard, D.; Coleman, J. N. Spray Deposition of Highly Transparent, Low-Resistance Networks of Silver Nanowires over Large Areas. *Small* **2011**, *7*, 2621–2628.

(30) Lili, L.; Dan, Y.; Le, W.; Wei, W. Electroless Silver Plating on The Pet Fabrics Modified with 3-Mercaptopropyltriethoxysilane. *J. Appl. Polym. Sci.* **2011**, *124*, 1912–1918.